Optical trapping in air on a single interference fringe

Aaron Schäpers, Olav Gaute Hellesø, Jochen Fick

Optical trapping in air on a single interference fringe

Aaron Schäpers[a], Olav Gaute Hellesø[b], Jochen Fick[a,*]

[a] *Université Grenoble Alpes, CNRS, Institut Neéel, 25 Avenue des Martyrs, 38000, Grenoble, France*
[b] *Department of Physics and Technology, UiT The Arctic University of Norway, Hansine Hansens veg 18, 9019, Tromsø, Norway*

Abstract

Stable and reproducible trapping in air of 1 μm and 500 nm dielectric particles has been realized using a dual beam optical fiber tweezers with cleaved commercial single mode fibers. The influence of the interference fringes of the two coherent and counter-propagating trapping beam is investigated by controlling the fringe visibility. Optical trapping on a series of up to 10 fringes or trapping on only one to two fringes has been observed in distinct experiments. High axial trapping efficiencies of up to 1 $\mathrm{nN}\cdot\mu\mathrm{m}^{-1}\mathrm{W}^{-1}$ is observed. The experimental results are supported by numerical simulations.

Keywords: optical tweezers, trapping in air, interference fringes, micro-particles

1. Introduction

Since its development in 1986 by Ashkin [1], optical tweezers have found many applications in different research domains such as biology, chemistry or physics. Most optical trapping experiments are done with particles in suspension. Optical trapping in air [2], and more recently in vacuum [3], is, however, of great interest.

Optical traps can, in most cases, be described by the harmonic oscillator model. Because of the high water viscosity, trapping in suspension corresponds to a heavily over-damped oscillator. Trapping in vacuum drastically reduce damping and allows to study light-matter interactions in more detail. The viscosity of air is about one order of magnitude lower than for water, but trapping in air still corresponds to an over-damped oscillator. However, the higher viscosity makes trapping in air more stable than in vacuum. In addition, the problem of particle heating is reduced.

In 1997 R. Omori *et. al.* trapped micrometer-sized glass spheres in air using a single beam tweezers [4]. A comparison between suspension and air tweezers showed that trapping in air requires significantly less optical power [5]. This fact is mainly due to the higher refractive index difference of, for example, polystyrene particles giving $\Delta n \approx 0.53$ in air instead of $\Delta n \approx 0.20$ in water.

*Corresponding author
Email address: jochen.fick@neel.cnrs.fr (Jochen Fick)

Previous works on optical trapping in air concerned mainly trapping of quite large dielectric particle in the 8 to 10 μm range [6, 7]. A micro-displacement sensor has been developed, using an optically trapped microprobe based on the interference scale [8]. In a different work, large, absorbing particles were trapped and transported in free space using standard diffraction lenses and using vortex or bottle beams [9, 10, 11]. Single dielectric and metallic micro and nanoparticles were trapped in air by L. Jauffred and S. Taheri using a trapping chamber designed to minimize any turbulence [12, 13]. In this context, the paramount influence of the surface of the trapped particle was revealed for gold nanoparticles [14].

In the field of meteorology, trapping in air was motivated by the study of droplet behavior inside clouds. Single and dual beam geometries were applied to micron-sized droplet trapping in air with focus on optical spectroscopic or micro-rheology studies to investigate droplet surface tension or particle viscosity [15, 16, 17, 18]. Furthermore, the spectroscopic characterization of fluorescent particles in air presents an interesting approach as it allows to eliminate all environmental influence of the surrounding medium [19, 20].

The first optical fiber tweezers was already realized in 1993 by Constable *et. al.* [21]. Their work represent perhaps the most straightforward optical trapping experiment as they used just two pigtailed lasers and realized fiber alignment by pushing them towards a capillary between two glass slides. Today, the use of nano-structured optical fibers allow very efficient trapping in single-fiber or dual-fiber geometries. In fact, one of the advantages of using optical fibers is that they facilitate the realization of dual beam tweezers. In this configuration, the constraints on beam focusing are significantly reduced as the scattering forces from the two beams cancel each other. Finally, as will be shown in the present paper, the possibility to trap on one single interference fringe results in high trapping efficiencies. Optical fiber based dual optical tweezers were used by different groups to trap water droplets or 3 - 5 µm dielectric particles [22, 23]

In this article, we investigate optical trapping in air by a dual fiber optical tweezers. The set-up is an adapted version of our suspension tweezers used for trapping and spectroscopic characterization of different kinds of nano-particles [24, 25, 26]. In contrast to former work, the best results are obtained with cleaved fibers instead of fiber tips or Fresnel lens fibers [27]. The influence of optical interference fringes will be studied in detail, both experimentally and using numerical simulations.

2. Methods

2.1. Experimental setup

A very compact and entirely fibered optical tweezers, fitting on a 750 x 450 mm breadboard, was developed (Fig. 1). A pigtailed diode-laser (λ = 808 nm, P_{max} = 250 mW) is coupled to a 2 × 2 fused fiber coupler. Each of its two outputs is connected to one of the trapping fibers. A variable attenuator in one light path allows to compensate for differences in transmission between the light paths. In the second light path, a three-paddle fiber polarization controller is introduced to adjust the relative polarization between the two trapping beams. For trapping, two cleaved, standard single mode fibers are used (Nufern, S630-HP)

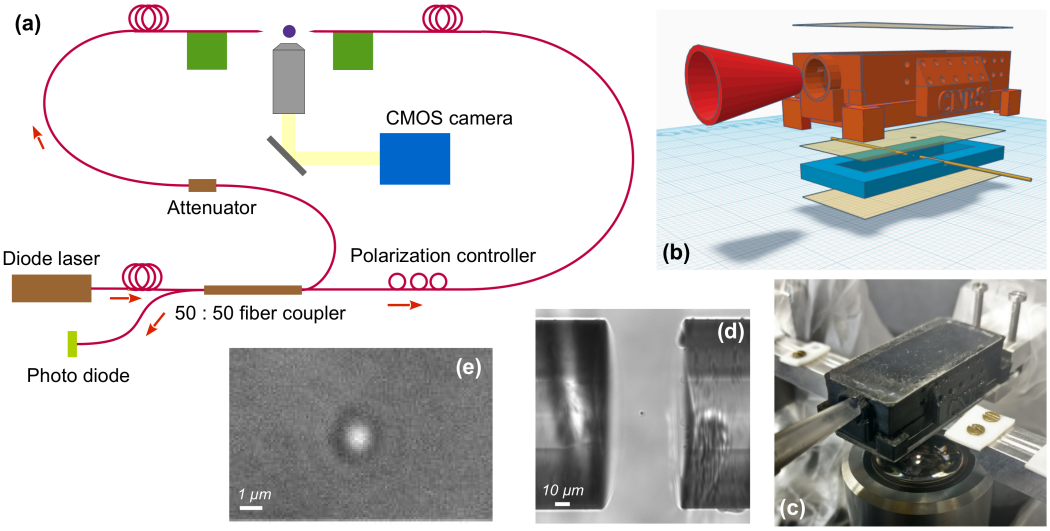

Figure 1: Optical fiber tweezers setup: (a) Schematic of the all-fibered tweezers, (b) CAD image of the trapping chamber: the upper compartment (brown), the lower chamber (blue), the two optical fibers (orange), the plastic films to seal and separate the compartments (yellow), and the nozzle for aerosol feeding (red). (c) Photo of the trapping chamber with the nozzle and the two optical fiber holders. (d) 1 μm polystyrene particle trapped between two cleaved fibers at 50 μm distance. (e) Same particle in a trapping video frame.

with a mean mode diameter of 4.2 μm and a numerical aperture of 0.12. Each fiber is fixed on a set of xyz piezoelectric translation stages for efficient fiber alignment.

Inspired by the work in Ref. [12, 13], an original two-compartment trapping chamber was designed and manufactured by 3D printing. It ensures effective particle feeding and shielding of trapped particles against any air draft (Fig. 1.b). A portable commercial nebulizer (Omron U22) is used to produce an aerosol from an ethanol suspension with microparticles. The aerosol is blown by means of a nozzle into the upper compartment of the trapping chamber ($10 \times 30 \times 7.5$ mm^3). Some droplets are then diffusing through a small hole ($\varnothing \approx 1$ mm) into the lower compartment which contains the optical trap ($h = 2$ mm). Once a droplet is trapped, the ethanol is quickly evaporating and the particle will remain trapped. The two trapping fibers are passing through opposite openings in the trapping chamber, with sufficiently large openings to allow alignment of the fibers. With this setup, trapping of a new particle is realized within less than ten minutes and particles remain trapped for a couple of hours.

2.2. Data acquisition and analysis

Videos of trapped particles are recorded at framerates of 1000 fps through a 50x long working distance microscope objective coupled to a CMOS camera. A homemade particle tracking algorithm in python is used to extract the time-dependent particle position in the $x - y$ observation plane. The video resolution is about 130 nm/pixel. By fitting over a number of pixels, the tracking algorithm has, however, an enhanced resolution of some picometers. The position records are then used to calculate the position probability P

independently in x and y directions for application of Boltzmann statistics in the framework of the equipartition theorem [24]. Supposing a harmonic trapping potential $U = 1/2\kappa x^2$, P can be written separately in x and y direction as:

$$P(\xi) = \frac{1}{Z} \cdot e^{\frac{-\kappa_\xi \cdot (\xi - \xi_0)^2}{k_b T}}, \tag{1}$$

with $\xi \in \{x, y\}$, Z the partition function, k_B the Boltzmann constant, T the absolute temperature, ξ_0 the mean position, and κ_ξ the trap stiffness. In the presence of interference fringes in the probability distribution in axial direction, $P(x)$ shows a series of n equidistant peaks and Eq. 1 can be modified to:

$$P_n(x) = A_0 \cdot e^{\frac{-\kappa_x^e \cdot (x - x_0^e)^2}{2k_B T}} \cdot \left\{ 1 - V * \left[1 - \sum_{j=0}^{n-1} e^{\frac{-\kappa_x^p \cdot (x - x_0^p - j \cdot \delta x)^2}{2k_B T}} \right] \right\} \tag{2}$$

with V the peak visibility factor, δx the peak (fringe) spacing, x_0^p the position of the first peak, and x_0^e the position of the Gaussian envelope function maximum. Two specific trap stiffnesses are defined: κ_x^e corresponding to trapping without interference fringes and κ_x^p corresponding to trapping on a single fringe. In our model κ_x^p is supposed to be the same for all observed peaks.

2.3. Numerical simulations

For nanoparticles, the Rayleigh approximation can be used to analytically find the optical force on a particle trapped by two counter-propagating Gaussian beams [28]. However, the particles used in this study are rather large for applying the Rayleigh approximation. Furthermore, the fibers have a mode radius $\omega_0 = 2.1$ μm, giving a Rayleigh length $z_0 = \pi\omega_0^2/\lambda = 17$ μm. The distances between the fibers considered here are $20 - 50$ μm. As this is just one or a few times the Rayleigh length, the Gaussian approximation for the beams cannot readily be justified. The finite element method is commonly used to simulate field distributions, but requires $5 - 10$ mesh-points per wavelength. This implies that a full 3D simulation of the problem becomes very memory-consuming. There are thus several obstacles for simulating the problem at hand, and also several paths that can be followed to simplify the problem. Initially, we tested a full finite element 3D simulation for a small separation between the fibers and also a quasi-3D model taking advantage of vertical and horizontal symmetries, thus simulating a quarter of the space. This is the same approach as has previously been used for trapping with counter-propagating beams in a gap between two planar optical waveguides [29]. Results from these accurate models were used to verify our simplified model.

By considering only particles on the optical axis, and only calculating forces along the optical axis, the problem has rotational symmetry around the optical axis. It can thus be simulated with the finite element method in 2D, taking into account the rotational symmetry. This is our choice for a simplified model as the memory requirements are low, it is fast to solve and it gave the same results as a full 3D-model for small separations between the fibers.

Mathematically, the force $\mathbf{F}$ with a full 3D-model is found by integrating the Maxwell stress tensor $\mathbf{T}$ and the surface normal $\hat{n}$ over the surface S of the sphere [30, 31]:

$$\mathbf{F} = \int_S \mathbf{T} \cdot \hat{n} \mathrm{d}s. \tag{3}$$

When simplifying to rotational symmetry, the expression becomes:

$$\mathbf{F} = 2\pi \int_L \mathbf{T} \cdot \hat{n} r \mathrm{d}l, \tag{4}$$

with L the line describing the sphere in 2D and r the radius to the line. For simplicity, the same symbols are used for the vectors and tensor $\mathbf{T}$ for 3D and 2D. As mentioned, applying rotational symmetry limits the study to particles on the axis and finding the force F_z along the axis. The 3D-model can handle any polarization through $\mathbf{T}$, while for the 2D model, the polarization must be out of the 2D plane. This corresponds to beams with parallel ($\Delta\phi = 0°$) polarization. For crossed polarization ($\Delta\phi = 90°$), the beams don't interfere and the force from one beam can be found independently of the force from the other beam. This makes it possible to find the force also for crossed polarization with a 2D model, but this is not considered in the following.

The finite element method (Comsol Multiphysics 6.0, RF-module) is used to find the optical mode of the trapping fibers. Using rotational symmetry, the field-distribution between the fibers is found for various positions of the particle. Both fibers are taken as sources with the fundamental mode and the same polarization (out of the plane, $\Delta\phi = 0°$). The polarization is thus parallel and the beams generate an interference pattern between the fibers. The axial force F_z on the particle is found with Equation 4 and using Comsol's definition of the Maxwell stress tensor. The integration is performed in post-processing, using built-in functions.

3. Experimental Results

In the present work, 500 nm and 1 μm commercial polystyrene particles are trapped at laser powers of $P = 24 - 66$ mW and fiber-to-fiber distances of $d = 20 - 50$ μm. In general, optical trapping of a single particle is realized in less than 10 minutes once the fibers are mounted and aligned. In the case of dual-beam optical tweezers with one single coherent light source, the two trapping beams are interfering and the resulting interference fringes have a significant influence on the behavior of the trapped particle. The visibility of the interference fringes can be controlled by rotating the polarization axis of one trapping beam. If the polarization axes of both beams are parallel, i.e. for zero polarization mismatch $\Delta\phi = 0$, the fringe visibility is maximal. On the other had, for crossed polarizations ($\Delta\phi = 90°$) no interference fringes are observed. In this case, the trapping efficiency is linearly increasing with optical power. For 1 μm particles and a fiber-to-fiber distance of $d = 50$ μm we measured a normalized trapping efficiency of $\tilde{\kappa}_x = 0.15$ pN$\cdot\mu$m$^{-1}\cdot$W^{-1} and $\tilde{\kappa}_y = 0.23$ pN$\cdot\mu$m$^{-1}\cdot$W^{-1} in axial (x) and transverse (y) directions, respectively. The transverse

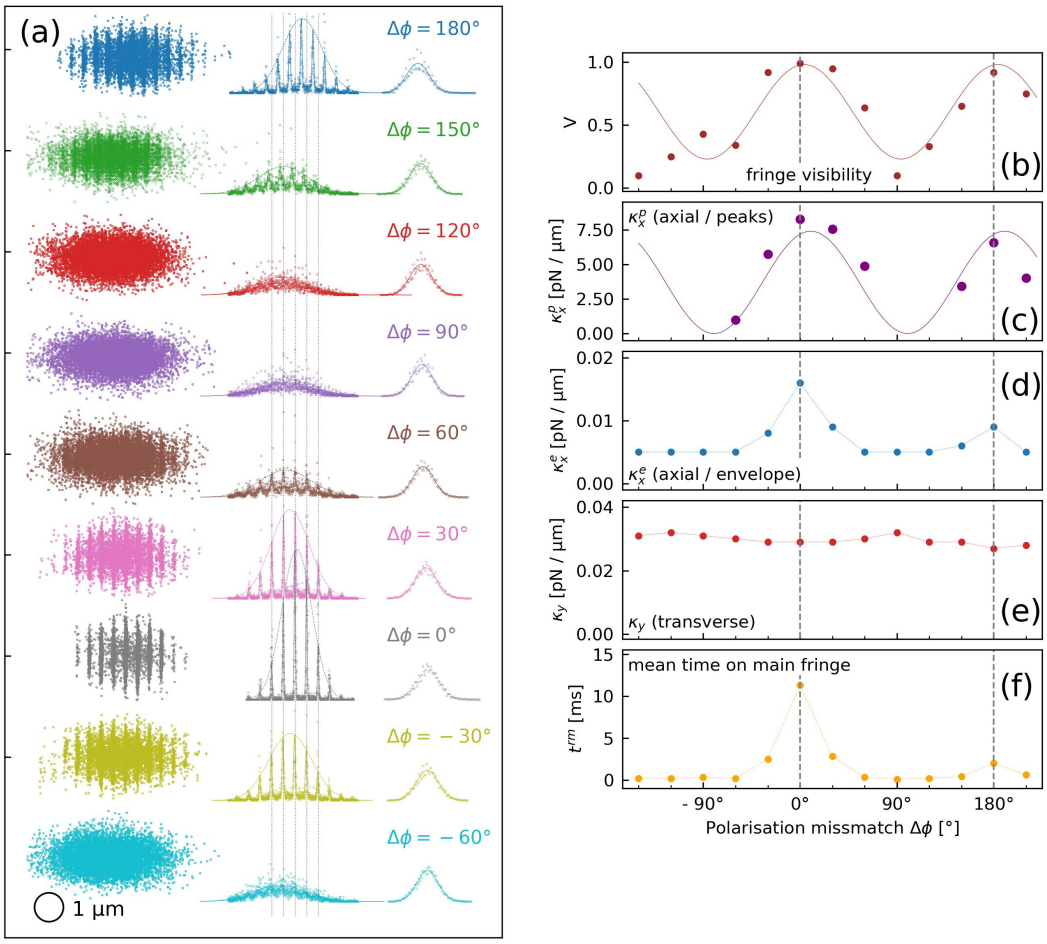

Figure 2: Optical trapping of a 1 μm particle on a series of interference fringes. (a) From left to right: 2D position tracking plots and position probabilities in axial (x) and transverse (y) directions for different polarization mismatches $\Delta\phi$. The black circle is an on scale sketch of the trapped particle. (b) - (f) Polarization mismatch dependence of indicated trapping parameters. The continuous lines in (a) and (b) are numerical fits, whereas the dotted lines in the other plots are guides to the eye.

trapping efficiency shows a $1/d^2$ dependency from the fiber-to-fiber distance, whereas the axial efficiency was found to be constant.

The influence of the interference fringes on the optical trapping is investigated by recording series of trapping videos of the same particle but with different polarization mismatches. The polarization of one beam is rotated in 30° steps over a 360° range. After the experiment, the zero polarization mismatch $\Delta\phi = 0°$ is found from the fringe visibility. The presented results correspond to the forward series ($0° \rightarrow 360°$). The backward series ($360° \rightarrow 0°$) shows similar results, but are not included here. The nominal fringe spacing, corresponding to $\lambda/2 = 404$ nm was used for fine-tuning the image resolution of ≈ 130 nm/pixel for each individual measurement series. For the following experimental series the laser power was fixed to $P = 66$ mW, with a fiber-to-fiber distance of $d = 50$ μm.

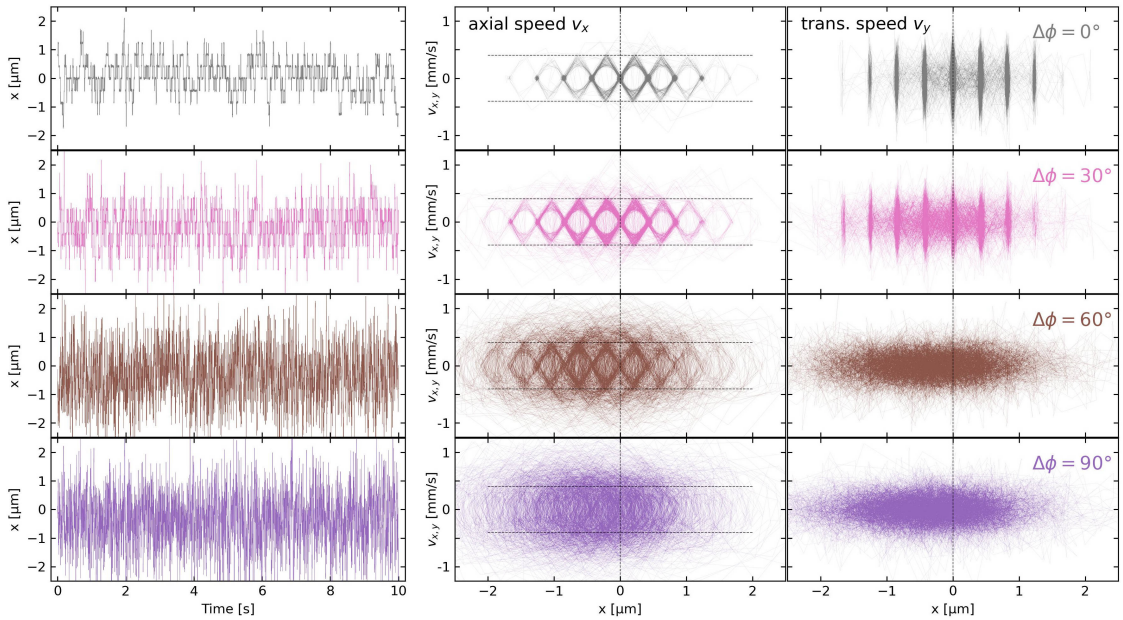

Figure 3: Axial particle dynamics for four polarization mismatches of the trapping series shown on Fig. 2. From left to right column: time-position records, axial speed (v_x) and transverse speed (v_y) as a function of the axial position (x). Horizontal dashed lines correspond to a speed of $v_x = \pm 404$ μm·s^{-1}.

3.1. Optical trapping on a series of interference fringes

Trapping of 1 μm polystyrene particles is found to be significantly influenced by the presence of the interference fringes (Fig. 2). For zero polarization mismatch, the positions corresponding to the interference fringes are well distinguishable in the particle position plots (Video 01 and Video 2). With increasing mismatch, the fringe visibility is decreasing and totally disappears for crossed polarizations ($\Delta\phi = 90°$). The fringes reappear with a second, but less prominent maxima at $\Delta\phi = 180°$. The lower fringe visibility at $\Delta\phi = 180°$ originates from the limits of our polarization controller. This device also slightly decreases the right beam intensity. Consequently, the mean trapping position and the interference fringe positions are shifted to the right for $\Delta\phi \gtrsim 150°$. For $\Delta\phi = -30°$ to $60°$ the fringe positions are stable, with some variation in the mean particle position.

The axial position probability records are fitted to Equation 2 by applying 10 peaks. The peak visibility V, shows a clear 180° periodicity with a maximum of $V = 99\%$ (Fig. 2.b). The peak trapping efficiency shows a maximum of $\kappa_x^p(0°) = 8.3$ pN·μm^{-1} (Tab. 1). The second maximum at 180° is lower with $\kappa_x^p(180°) = 6.6$ pN·μm^{-1} (Fig. 2.c). The envelope trapping efficiency is about 600 times smaller and shows a similar dependence with two maxima of $\kappa_x^e(0°) = 16$ fN·μm^{-1} and $\kappa_x^e(180°) = 9$ fN·μm^{-1}. Trapping in transverse direction is not affected by the polarization mismatch change and is quasi-stable with a mean efficiency of $\tilde{\kappa}_y = 30$ fN·μm^{-1} (Fig. 2.e). The mean time the particle is trapped on the main peak shows a sharp maximum of $\tilde{t}_r = 11.3$ ms at $\Delta\phi = 0°$. Besides this peak, $\tilde{t}_r$ is in the range 0.2 to 0.3 ms.

We now turn to the analysis of the trapping dynamics, i.e. the time dependent position

Table 1: Main optical trapping efficiency parameters: κ_x^e, κ_x^p axial envelope and peak stiffnesses, κ_y transverse stiffness, and $\tilde{t}_r$ mean remaining time on main peak ($P = 66$ mW, total recording time: 10 s).

	1 μm particle		500 nm particle	
	1. series	2. series		
κ_x^e	0.016^a	–	0.010^b	[pN·μm^{-1}]
κ_x^p	8.3^a	65^a	5.5^a	[pN·μm^{-1}]
$\tilde{\kappa}_y$	0.030^b	0.37^b	0.066^b	[pN·μm^{-1}]
$\tilde{t}_r$	11.3^a	$10\ 000^a$	1.7^a	[ms]
nbr peaks	10	1 – 3	9	

^{a}maximum value, ^{b}mean value

and the particle speed. The axial position x(t) for four polarizations is shown on Fig. 3. For $\Delta\phi = 0°$ the particle is "hopping" between discrete positions. With increasing polarization mismatch, this effect is disappearing, resulting in a random motion for orthogonal beams. This effect is more pronounced when looking at the position-dependent particle speed. The most interesting feature concerns the axial distribution of the axial speed $v_x(x)$. The plot, shaped as an eye-diagram, suggests that the particle is hopping directly from one fringe to the neighbor during a single video frame interval, resulting in an transfer speed of $v_x^t \approx 404$ μm·s^{-1} (dotted horizontal lines in Figure 3). For larger polarization mismatch and less efficient trapping on the fringes, the eye-diagram is getting less pronounced. The influence of the interference fringes remains, however, visible for $\Delta\phi = 90°$. The influence of the polarization mismatch on the transverse speed distribution $v_y(x)$ is less pronounced. For zero polarization mismatch, the maximum transverse speed v_y is slightly higher than v_x and decreases with increasing $\Delta\phi$.

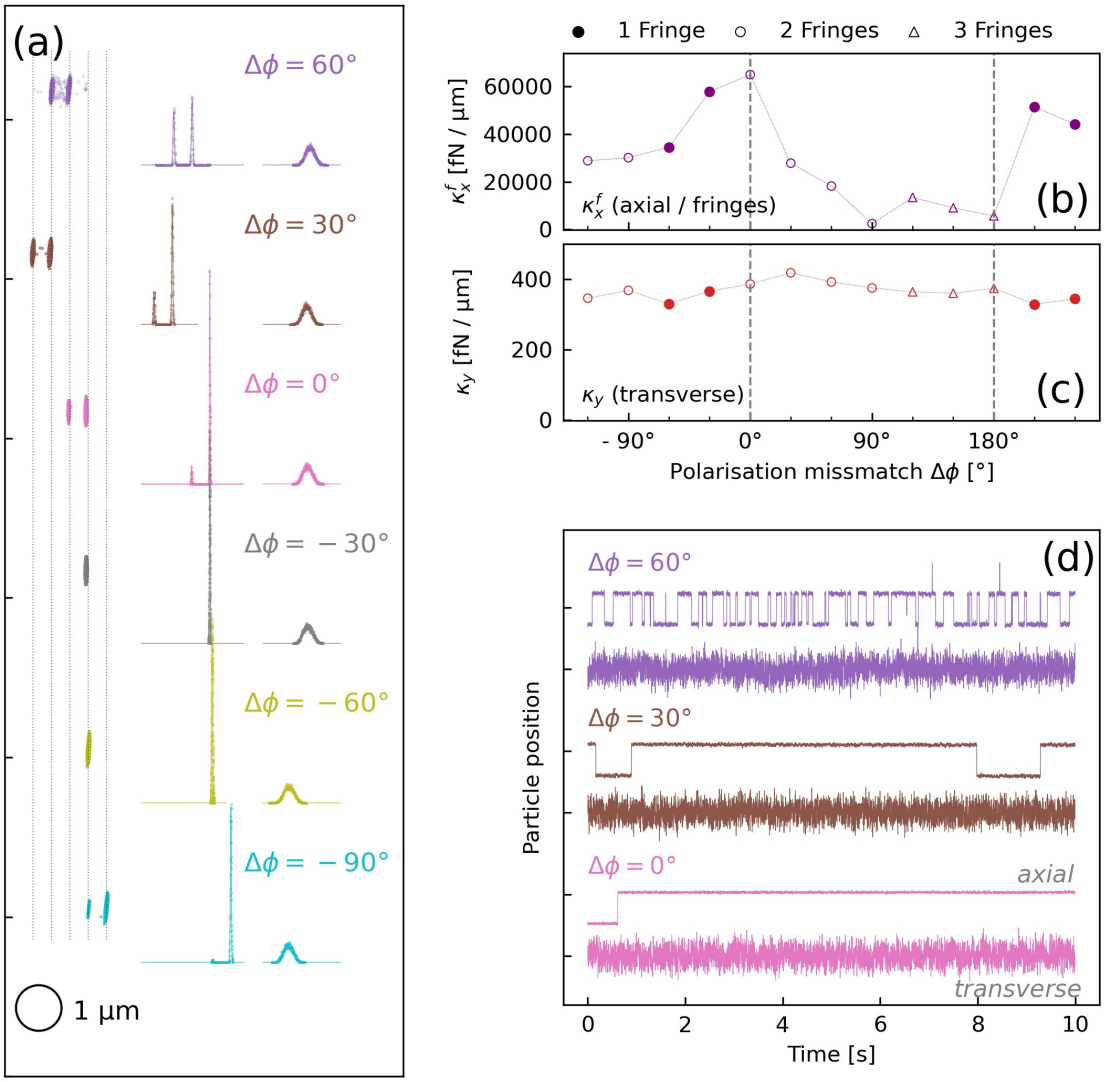

Figure 4: Optical trapping of a 1 μm particle on one to three fringes. (a) 2D position tracking plots and position probabilities in axial (x) and transverse (y) directions for different polarization mismatches $\Delta\phi$. The black circle is an on scale sketch of the trapped particle. Axial peak (b) and transverse trap stiffness (c). The dotted lines are guides to the eye. (d) Axial and transverse time position records for three polarization mismatches.

3.2. Optical trapping on few interference fringes

A different effect is observed in a subsequent optical trapping experiment with identical conditions, but improved fiber alignment. In this series, the particle is actually trapped on a single, or up to three interference fringes (Fig. 4). For the different videos the particle is trapped on five uniformly spaced interference fringes. Even in the case of $\Delta\phi = 90°$, the imperfect polarization of the beams results in trapping on only two interference fringes.

Depending on the number of peaks, the trapping efficiency was obtained by fitting the data to Equation 1 or 2. Here, the envelope trap stiffness has no physical meaning and

becomes a free fitting parameter. The maximum axial peak trapping stiffness of $\kappa_x^p = 65$ pN$\cdot\mu$m^{-1} is about eight time larger than for the first series. The polarization mismatch dependency is, however, less pronounced with no clear minimum or 180° periodicity (Fig. 4.b). In the transverse direction, the trapping efficiency is quite constant with a mean value of $\kappa_y = 0.037$ pN$\cdot\mu$m^{-1}, about ten times higher than in the first series.

The highest trapping efficiency is observed for a sequence with trapping on two interference fringes, and not for trapping on a single fringe as expected. During the 10 s of the sequence, the particle is, however, hopping only once between two fringes (Fig. 4.d, $\Delta\phi = 0°$). For $\Delta\phi = 30°$, the particle is already moving between the fringes four times and at $\Delta\phi = 60°$, the particle is hopping more than 30 times. Whether the particle is trapped on one or two fringes can therefore be regarded as a statistical coincidence. Moreover, it is random which specific fringe the particle is trapped on.

3.3. Optical trapping of 500 nm particles

A similar trapping behavior is observed for optical trapping of 500 nm particles, including experiments with trapping on several fringes and experiments with trapping on only one to three fringes. These results will not be reported in detail as they do not provide fundamentally new insight into the underlying physics. The main results are summarized in Table 1. Optical trapping is observed on 9 interference fringes with a maximum axial on-fringe trap stiffness of $\kappa_x^p(\Delta\phi = 0°) = 5.5$ pN$\cdot\mu$m^{-1}, which is of the same order as for the 1 μm particles. In the transverse direction, the mean trap stiffness is $\bar{\kappa}_y = 0.066$ pN$\cdot\mu$m^{-1}, which is twice the value for 1 μm particles. A significant difference is observed for the mean time on the main fringe $\tilde{t}_r = 1.7$ ms, which is ten times shorter and reflects the general observation of less stable trapping for 500 nm particles.

3.4. Numerical simulations

Numerical simulations were performed to mimic the experimental trapping of 1 μm polystyrene particles, two cleaved fibers at a distance of ≈ 50 μm and an optical power of $P = 66$ mW in each fiber. The high index difference between the polystyrene particle and air leads to strong light scattering with three to four interference fringes inside the particle volume (Fig. 5a). The calculated optical force for parallel optical polarization ($\Delta\phi = 0°$) is shown in Figure 5b. The periodic oscillations are attributed to the interference fringes. The three chosen fiber distances are $(i + \delta) \cdot \lambda$ with $\lambda = 808$ nm, $i = 62$, and $\delta \in \{0, \frac{1}{4}, \frac{1}{2}\}$, close to the experimental value of $d = 50$ μm. The higher force for $\delta = \frac{1}{2}$ is due to higher light intensity inside the Fabry-Pérot type cavity which is formed between the two cleaved fibers.

The trapping potential U is calculated by integrating the optical force (inset Fig. 5.b). It shows the superposition of the parabolic (harmonic) potential of a two incoherent beam tweezers with the periodic modulation caused by the interference fringes. The potential well between two adjacent minima is very high, above $\approx 100 \cdot k_B T$. For better comparison with the experimental results, the position probability was calculated using $P = \frac{1}{Z} \exp(U/2k_B T)$ (Fig. 5.c). Under these conditions, optical trapping is limited to trapping on the two central interference fringes. The comparison with the experimental curve for $\Delta\phi = 0°$ is very good.

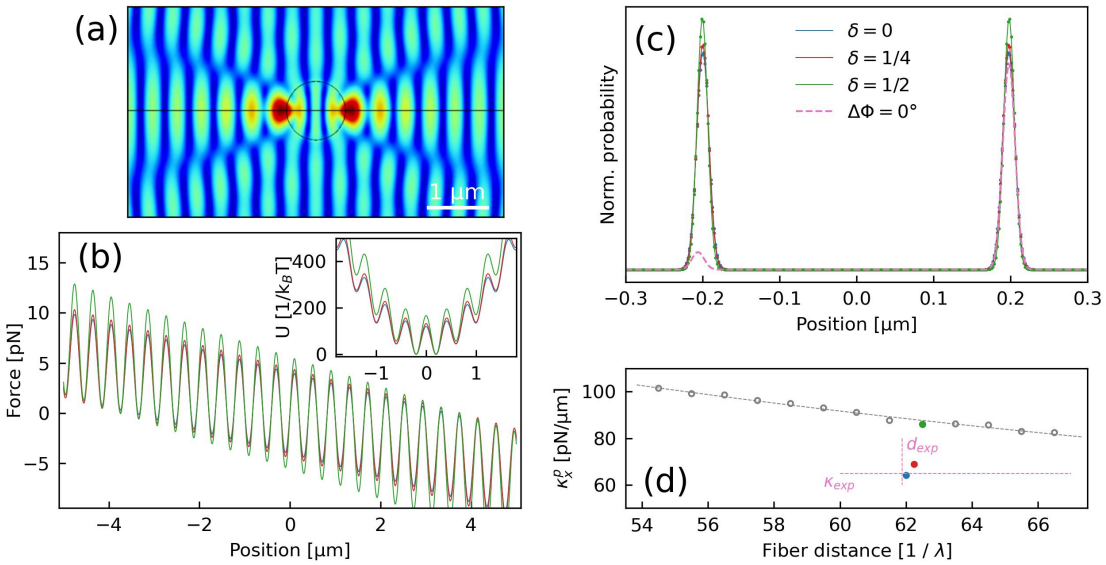

Figure 5: (a) 2D map of the electrical light field norm showing the strong light scattering of the trapped particle. (b) Calculated axial optical force at $P = 66$ mW on a 1 μm particle between two cleaved fibers for three distances $d = (62 + \delta) \cdot \lambda$ as labeled in (c) ($\Delta\phi = 0$, $P = 50$ mW). Inset: Corresponding potential U. (c) Calculated position probability (dots) and numerical fits as used for the experimental data. (d) Calculated axial peak trap stiffness as a function of the fiber distance (gray circles all $\delta = 0$, color dots as labeled in (c)). The experimental result for $\Delta\phi = 0$ (Fig. 4) is added as pink lines in (c) and (d).

Experimentally, the occupation rate is not equal. This is because the particle is initially trapped on one fringe and only moves to the second one at the end of the observation time.

The axial peak trap stiffness is obtained from the calculated position distribution applying the same numerical fitting approach as for the experimental data (Fig. 5.d). The constant decrease of κ_x^p with increasing fiber distance can be approximated by a $1/d^2$ dependence. Moreover, the trapping stiffness is enhanced by 30% for $\delta = \frac{1}{2}$ with respect to $\delta = 0$. To observe this enhancement experimentally, a very precise angular alignment of the two fibers is required, with perfectly cleaved end-faces. These conditions are quite difficult to realize experimentally.

4. Discussion

Optical trapping with two counter-propagating, weakly diverging laser beams results in general in an anisotropic trapping potential. Trapping in the transverse direction has been observed to be about three times more efficient than in the axial direction [24, 25]. In the case of converging beams, this anisotropy is even more pronounced [27]. Trapping in the transverse direction is dominated by the gradient force, which pulls the particle towards the beam center, and the forces created by the two beams are adding up. The highest trapping efficiency is obtained for beam waists close to the particle size. In the axial direction, particles are pushed by the scattering force. The forces created by the two beams are opposing each other. Diverging or focused beams, namely with varying intensity, are required to obtain a

stable axial trapping position.

The single mode optical fibers used here have a mode diameter of $\omega = 4.2$ μm and a numerical aperture of NA = 0.12. Thus, the large beam diameter explains the relatively low transverse trapping efficiency, whereas the weak beam divergence results in a low axial envelope trapping efficiency. In previous experiments in air, we have used fiber tips with beam parameters better adapted to the particles, with $\omega = 0.9$ μm and NA = 0.26. It was, however, impossible to trap particles with these fiber tips. In fact, the stronger beam divergence resulted in larger transverse scattering forces, prohibiting the particles from reaching the stable optical trapping region.

In the present case of weakly diverging and coherent beams, the sum of the opposing scattering forces is relatively small and the optical gradient force related to the interference fringes dominates. Thus, trapping on one single fringe can be realized. This on-fringe trapping is of great fundamental and experimental interest as the light intensity gradient of an interference fringe is the steepest possible gradient in the optical far field.

For the highest observed trapping efficiency of 65 pN$\cdot\mu$m^{-1}, the axial position probability peak width (FWHM) is 19 nm, about seven times smaller than the resolution given by the camera pixel size, and 50 times smaller than the particle size. We estimate that this value is near the experimental resolution of our set-up. On the other hand, a very good agreement of the experimental results with the numerical simulations is observed. The possibility of trapping on one or two interference fringes was predicted by the simulations and shown experimentally. Also, the simulated and measured trapping efficiencies correspond well.

For particle trapping in suspension, we have previously observed similar on-fringe trapping, but only for 300 nm particles and with considerably lower visibility [25]. In fact, several conditions are required for on-fringe trapping. First, the particle diameter should be similar to, or smaller than, the fringe spacing to have only a few fringes "inside" the particle. For example at 808 nm wavelength, three or four fringes are inside a 1 μm particle. Secondly, in order to have a significant gradient force, a high index difference between the particle and the surroundings is essential. For a polystyrene particle in air, $\Delta n_{air} = 0.57$, which is more than twice that in water ($\Delta n_{water} = 0.25$). Finally, for small particles, Brownian motion becomes dominant and prevents single fringe trapping.

Using a focused laser beam, a normalized trapping stiffness of $\bar{\kappa} = 16$ pN$\cdot\mu$m$^{-1}\cdot$W^{-1} was reported for 1 μm silica particles [13]. This value is about eight times higher than the transverse stiffness observed here, but 60 times lower than the normalized peak trapping stiffness of $\bar{\kappa}_x^p = 985$ pN$\cdot\mu$m$^{-1}\cdot$W^{-1}.

5. Conclusion

Stable and reproducible optical trapping of micron-sized dielectric particles in air was realized using our dual beam fiber optical tweezers. The geometry of this tweezers set-up is straightforward, with two commercial cleaved single-mode optical fibers, a commercial nebulizer, a 3D-printed trapping chamber and a homemade microscope. The optics path from the pigtailed laser to the trapping fibers is entirely fibered, thus resulting in a very low footprint.

Depending on the alignment conditions, trapping on a series of interference fringes or on a single interference fringe is observed. A very high trapping efficiency of up to $\kappa_x^p = 65$ pN$\cdot\mu$m^{-1} is observed for a low light power of 66 mW. The paramount influence of the interference fringes is elucidated by controlling the polarization mismatch of the two trapping beams and thus gradually suppressing the fringe visibility.

The results presented in this article show that dual fiber optical tweezers allow us highly efficient trapping of micron-sized objects in a compact set-up using the extremely steep intensity gradient that occurs from the interference fringes of two coherent laser beams. Our set-up could be easily modified to integrate spectroscopic characterization of the trapped particles.

Acknowledgments

We thank M. Fick for his contribution in designing and fabricating the optical trapping chamber. J.Fick acknowledges funding from Agence Nationale de la Recherche (project no. ANR-16-CE24-0014-01) whereas O.G. Hellesø acknowledges support from the Research Council of Norway (grant no. 302333).

References

[1] A. Ashkin, J. M. Dziedzic, J. E. Bjorkholm, S. Chu, Observation of a single-beam gradient force optical trap for dielectric particles, Opt. Lett. 11 (1986) 288.

[2] Z. Gong, Y.-L. Pan, G. Videen, C. Wang, Optical trapping and manipulation of single particles in air: Principles, technical details, and applications, J. Quant. Spec. Rad. Trans. 214 (2018) 94–119. doi:10.1016/j.jqsrt.2018.04.027.

[3] J. Millen, T. S. Monteiro, R. Pettit, A. N. Vamivakas, Optomechanics with levitated particles, Rep. Prog. Phys. 83 (2020) 026401. doi:10.1088/1361-6633/ab6100.

[4] R. Omori, T. Kobayashi, A. Suzuki, Observation of a single-beam gradient-force optical trap for dielectric particles in air, Opt. Lett. 22 (1997) 816–818.

[5] M. D. Summers, D. R. Burnham, D. McGloin, Trapping solid aerosols with optical tweezers: A comparison between gas and liquid phase optical traps, Opt. Express 16 (2008) 7739–7747. doi:10.1364/OE.16.007739.

[6] M. Michihata, T. Yoshikane, T. Hayashi, Y. Takaya, New technique for single-beam gradient-force laser trapping in air, Int. J. Optomechatron. 7 (2013) 46–59. doi:10.1080/15599612.2012.760122.

[7] R. Kampmann, A. K. Chall, R. Kleindienst, S. Sinzinger, Optical system for trapping particles in air, Appl. Opt. 53 (2014) 777–784. doi:10.1364/AO.53.000777.

[8] M. Michihata, T. Hayashi, D. Nakai, Y. Takaya, Microdisplacement sensor using an optically trapped microprobe based on the interference scale, Rev. Sci. Instr. 81 (2010) 015107. doi:10.1063/1.3292684.

[9] V. Shvedov, A. Desyatnikov, A. Rode, Y. Izdebskaya, W. Krolikowski, Y. Kivshar, Optical vortex beams for trapping and transport of particles in air, Appl. Phys. A 100 (2010) 327.

[10] V. G. Shvedov, C. Hnatovsky, A. V. Rode, W. Krolikowski, Robust trapping and manipulation of airborne particles with a bottle beam, Opt. Express 19 (2011) 17350–17356.

[11] P. Zhang, Z. Zhang, J. Prakash, S. Huang, D. Hernandez, M. Salazar, D. N. Christodoulides, Z. Chen, Trapping and transporting aerosols with a single optical bottle beam generated by moiré techniques, Opt. Lett. 36 (2011) 1491–1493. doi:10.1364/OL.36.001491.

[12] S. M.-R. Taheri, M. Sadeghi, E. Madadi, S. N. S. Reihani, Tube length-assisted optimized aerosol trapping, Opt. Commun. 329 (2014) 196–199. doi:10.1016/j.optcom.2014.05.022.

[13] L. Jauffred, S. M.-R. Taheri, R. Schmitt, H. Linke, L. B. Oddershede, Optical Trapping of Gold Nanoparticles in Air, Nano Lett. 15 (2015) 4713–4719. doi:10.1021/acs.nanolett.5b01562.
[14] Y. Arita, G. Tkachenko, N. McReynolds, N. Marro, W. Edwards, E. R. Kay, K. Dholakia, Invited article: Optical trapping of ultrasmooth gold nanoparticles in liquid and air, APL Photon. 3 (2018) 070801. doi:10.1063/1.5030404.
[15] D. McGloin, D. R. Burnham, M. D. Summers, D. Rudd, N. Dewar, S. Anand, Optical manipulation of airborne particles: techniques and applications, Faraday Discuss. 137 (2008) 335–350. doi:10.1039/b702153d.
[16] M. Guillon, B. Stout, Optical trapping and binding in air: Imaging and spectroscopic analysis, Phys. Rev. A 77 (2008) 023806. doi:10.1103/PhysRevA.77.023806.
[17] O. Brzobohatý, M. Šiler, J. Ježek, P. Jákl, P. Zemánek, Optical manipulation of aerosol droplets using a holographic dual and single beam trap, Opt. Lett. 38 (2013) 4601–4604.
[18] R. M. Power, J. P. Reid, Probing the micro-rheological properties of aerosol particles using optical tweezers, Rep. Prog. Phys. 77 (2014) 074601.
[19] C. Wang, Y.-L. Pan, G. Videen, Optical trapping and laser-spectroscopy measurements of single particles in air: a review, Meas. Sci. Technol. 32 (2021) 102005. doi:10.1088/1361-6501/ac0acf.
[20] M.-Y. Wu, D.-X. Ling, L. Ling, W. Li, Y.-Q. Li, Stable optical trapping and sensitive characterization of nanostructures using standing-wave raman tweezers, Sci. Rep. 7 (2017) 4293. doi:10.1038/srep42930.
[21] A. Constable, J. Kim, J. Mervis, F. Zarinetchi, M. Prentiss, Demonstration of a fiber-optical light-force trap, Opt. Lett. 18 (1993) 1867–1869. doi:10.1364/OL.18.001867.
[22] D. Rudd, C. Lopez-Mariscal, M. Summers, A. Shahvisi, J. C. Gutiérrez-Vega, D. McGloin, Fiber based optical trapping of aerosols, Opt. Express 16 (2008) 14550–14560.
[23] G. Xiao, T. Kuang, W. Xiong, X. Han, H. Luo, A pzt-assisted single particle loading method for dual-fiber optical trap in air, Opt. Laser Technol. 126 (2020) 106115. doi:10.1016/j.optlastec.2020.106115.
[24] J.-B. Decombe, S. Huant, J. Fick, Single and dual fiber nano-tip optical tweezers: trapping and analysis, Opt. Express 21 (2013) 30521–30531. doi:10.1364/OE.21.030521.
[25] J.-B. Decombe, F. J. Valdivia-Valero, G. Dantelle, G. Lemenager, T. Gacoin, G. Colas des Francs, S. Huant, J. Fick, Luminescent nanoparticle trapping with far-field optical fiber-tip tweezers, Nanoscale 8 (2016) 5334–5342. doi:10.1039/C5NR07727C.
[26] A. Kumar, A. Asadollahbaik, J. Kim, K. Lahlil, S. Thiele, A. M. Herkommer, S. N. Chormaic, J. Kim, T. Gacoin, H. Giessen, J. Fick, Emission spectroscopy of nayf4:eu nanorods optically trapped by Fresnel lens fibers, Photon. Res. 10 (2022) 332–339. doi:10.1364/PRJ.434645.
[27] A. Asadollahbaik, S. Thiele, K. Weber, A. Kumar, J. Drozella, F. Sterl, A. Herkommer, H. Giessen, J. Fick, Highly efficient dual-fibre optical trapping with 3d printed diffractive fresnel lenses, ACS Photonics 7 (2020) 88–97.
[28] P. Zemánek, A. Jonáš, L. Šrámek, M. Liška, Optical trapping of rayleigh particles using a gaussian standing wave, Opt. Commun. 151 (1998) 273–285. doi:10.1016/S0030-4018(98)00093-5.
[29] O. G. Hellesø, P. Løvhaugen, A. Z. Subramanian, J. S. Wilkinson, B. S. Ahluwalia, Surface transport and stable trapping of particles and cells by an optical waveguide loop, Lab on a Chip 12 (2012) 3436–3440. doi:10.1039/C2LC40375G.
[30] S. Gaugiran, S. Gétin, J. M. Fedeli, G. Colas, A. Fuchs, F. Chatelain, J. Dérouard, Optical manipulation of microparticles and cells on silicon nitride waveguides, Opt. Express 13 (2005) 6956–6963. doi:10.1364/OPEX.13.006956.
[31] M. Dienerowitz, M. Mazilu, K. Dholakia, Optical manipulation of nanoparticles: a review, J. Nanophot. 2 (2008) 021875. doi:10.1117/1.2992045.